Postdeposition annealing on RF-sputtered $SrTiO_3$ thin films

Türkan Bayrak, Seda Kizir, Enver Kahveci, Necmi Bıyıklı, and Eda Goldenberg

Citation: Journal of Vacuum Science & Technology A **35**, 021505 (2017); doi: 10.1116/1.4973970
View online: https://doi.org/10.1116/1.4973970
View Table of Contents: http://avs.scitation.org/toc/jva/35/2
Published by the American Vacuum Society

Articles you may be interested in

Evolution of microstructure and macrostress in sputtered hard Ti(Al,V)N films with increasing energy delivered during their growth by bombarding ions
Journal of Vacuum Science & Technology A: Vacuum, Surfaces, and Films **35**, 020601 (2017); 10.1116/1.4967935

Electric potential screening on metal targets submitted to reactive sputtering
Journal of Vacuum Science & Technology A: Vacuum, Surfaces, and Films **35**, 021307 (2017); 10.1116/1.4972566

Contrasting transparent conductive properties of ZnO films on amorphous and crystalline substrates in view of thickness dependence
Journal of Vacuum Science & Technology A: Vacuum, Surfaces, and Films **35**, 021503 (2017); 10.1116/1.4973540

Maximizing stoichiometry control in reactive sputter deposition of TiO_2
Journal of Vacuum Science & Technology A: Vacuum, Surfaces, and Films **35**, 020606 (2017); 10.1116/1.4974140

Industrial-scale sputter deposition of molybdenum oxide thin films: Microstructure evolution and properties
Journal of Vacuum Science & Technology A: Vacuum, Surfaces, and Films **35**, 021504 (2017); 10.1116/1.4973214

Experimental and numerical investigations on time-resolved characteristics of pulsed inductively coupled O_2/Ar plasmas
Journal of Vacuum Science & Technology A: Vacuum, Surfaces, and Films **35**, 021301 (2017); 10.1116/1.4967913

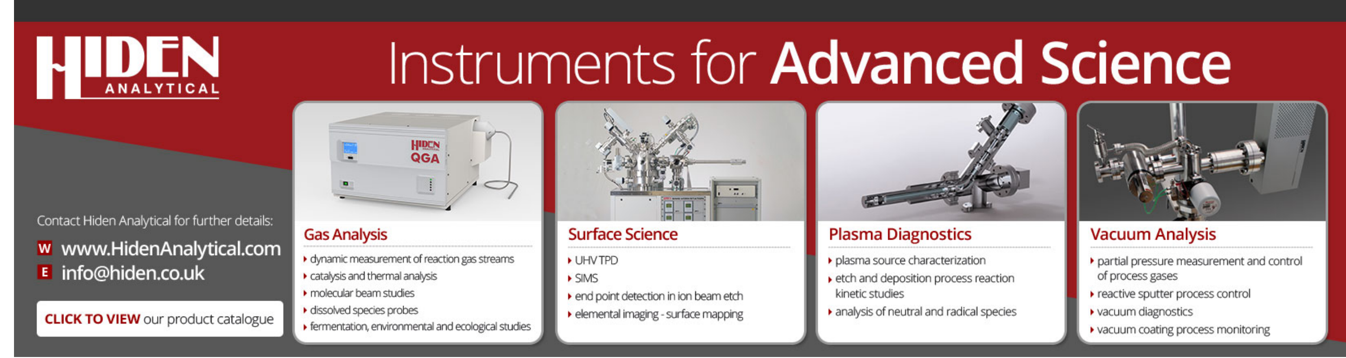

Postdeposition annealing on RF-sputtered $SrTiO_3$ thin films

Türkan Bayrak, Seda Kizir, Enver Kahveci, and Necmi Bıyıklı
National Nanotechnology Research Center (UNAM), Bilkent University, Ankara 06800, Turkey and Institute of Materials Science and Nanotechnology, Bilkent University, Ankara 06800, Turkey

Eda Goldenberg[a)]
Department of Physics, Advanced Research Laboratories, Bilkent University, 06800 Ankara, Turkey

(Received 18 August 2016; accepted 28 December 2016; published 10 January 2017)

Understanding of structural, optical, and electrical properties of thin films are very important for a reliable device performance. In the present work, the effect of postdeposition annealing on stoichiometric $SrTiO_3$ (STO) thin films grown by radio frequency magnetron sputtering at room temperature on *p*-type Si (100) and quartz substrates were studied. Highly transparent and well adhered thin films were obtained in visible and near infrared regions. As-deposited films were amorphous, while nanocrystalline and polycrystalline phases of the STO thin films formed as a function of annealing temperature. Films annealed at 300 °C showed nanocrystallinity with some amorphous phase. Crystallization started after 15 min annealing at 700 °C, and further improved for films annealed at 800 °C. However, crystallinity reduced for films which were annealed at 900 °C. The optical and electrical properties of STO thin films affected by postdeposition annealing at 800 °C: E_g values decreased from 4.50 to 4.18 eV, $n(\lambda)$ values (at 550 nm) increased from 1.81 to 2.16. The surface roughness increased with the annealing temperature due to the increased crystallite size, densification and following void formation which can be seen from the scanning electron microscopy images. The highest dielectric constants (46 at 100 kHz) observed for films annealed at 800 °C; however, it was lower for 300 °C annealed (25 at 100 kHz) and as-deposited (7 at 100 kHz) STO films having ~80 nm thickness. © *2017 American Vacuum Society*.
[http://dx.doi.org/10.1116/1.4973970]

I. INTRODUCTION

Ferroelectric oxides as thin-films or heterostructures are essential components in a wide variety of applications, including microelectronics, nonlinear optics, sensors and actuators, or multifunctional combinations of each application including tunable microwave device,[1,2] gate oxide insulator,[3,4] memory applications,[4–10] and optical elements.[11–14] They have received considerable attention owing to their small volume of capacitance with high dielectric constant, low dielectric loss, and switching polarization mechanism.[5,6] However, the challenges with ferroelectric material fabrication and the understanding the material properties banned the attempts to make practical memory devices until the 1980s.[15] Today, ferroelectric materials can be fabricated in novel geometries such as nanostructures due to the progress in fabrication techniques and remaining ferroelectric characteristics sizes up to as small as 20 nm.[16,17] Among various oxide ferroelectric materials, $SrTiO_3$ (STO) is an attractive thin film material due to the low dielectric loss at cryogenic temperatures, high dielectric constant, and excellent optical transparency in visible and near infrared regions.

In recent years, considerable effort has been directed toward the deposition of STO thin films and the optimization of deposition parameters for the improved film properties. Growth of STO thin films by various techniques have already been described in the literature.[18–22] High quality films of STO can be deposited at elevated temperatures (500–1000 °C), whereas low-temperature deposition methods are needed for next generation device applications including CMOS-compatible device integration and potential durable flexible optoelectronics. Low temperature deposition of STO and the temperature dependent properties, regarding film microstructure, have not been discussed in terms of electrical and optical characteristics. In addition, there is a limited work on the impact of postdeposition annealing on STO thin films grown via radio frequency (RF)-magnetron sputtering at room temperature (RT) using Si and quartz substrates.[18]

In the present paper, the effects of the postdeposition annealing temperature on the physical characteristics of STO thin films deposited using radio frequency (RF) magnetron sputtering were systematically investigated. In addition to the determination of the film microstructure, and of the optical constants (n and k) the variation of the film dielectric constant, dielectric losses are specifically addressed. In a broader sense, the study of the effects of annealing temperature on the structure, composition, morphology, and the electrical characteristics of the films allows us to better assess the film behavior.

II. EXPERIMENTAL METHODOLOGY

A. Film deposition

Stoichiometric and uniform STO thin films were grown at RT by off-plane axis VAKSIS NanoD–4S RF-magnetron sputtering system in a pure argon environment. The base pressure of the chamber was lower than 6.5×10^{-6} Torr (0.87 mPa). Film depositions were performed using a stoichiometric

a)Electronic mail: edacetinorgu@gmail.com

$SrTiO_3$ ceramic target (50 mm, purity 99.9%). For all experiments, target to sample distance was settled to 5 cm, and depositions were performed at a constant pressure of 0.93 Pa. Prior to the deposition, *p*-type Si(100) and quartz substrates were cleaned sequentially in acetone and isopropanol with final rinsing in deionized water. To evaluate the effect of postdeposition annealing on film microstructure, morphology, optical and electrical properties, films were annealed at five different temperatures (300, 600, 700, 800, and 900 °C) for 1 h in O_2 ambient (200 sccm) using ATV-Unitherm (RTA SRO-704) rapid thermal annealing system. In addition to the effect of temperature, time dependent annealing for 15, 30, and 45 min were performed at 700 °C since the polycrystalline phase formation was started at this temperature. Heating rate was ~3.5 °C/s, and samples were taken out from the annealing chamber after the system was cooled down to below 80 °C. For ease of discussion, samples were labeled as STO-RT, STO-300, STO-600, STO-700, STO-800, STO-900, and STO-700/15, STO-700/30, STO-700/45, respectively. The summary of the film deposition and postdeposition annealing conditions is given in Table I.

B. Film characterization

Grazing-incidence x-ray diffraction (GIXRD) measurements were carried out via PANalytical X'Pert PRO MRD system using Cu-K_α (1.5406 Å) radiation with 0.3° angle of incidence for the examination of the structural characteristics of STO films. GIXRD patterns were recorded in the range of 20°–90° with a step size and counting time of 0.1° and 10 s, respectively. Peak positions and the crystallite size values were obtained by fitting the GIXRD data using PANALYTICAL X'PERT HIGHSCORE PLUS software. Lattice parameters, volume, and crystallite sizes of the annealed films were extracted from Rietveld refinement and Williamson-Hall plot methods using PANALYTICAL X'PERT HIGHSCORE PLUS software, respectively.[23–26]

FEI Tecnai G2 F30 transmission electron microscope (TEM) system operating at a voltage under 300 kV was used for HR-TEM analysis of the crystal structure. Samples for TEM measurements were prepared by focus ion beam (FIB) (FEI Vion Plasma FIB) at an acceleration voltage of 30 kV, using different beam currents in the range of 50 pA to 6.5 nA. Damaged layers which formed between the film and substrate interfaces were removed by FIB milling at reduced beam voltages of 5 kV. For obtaining selected area diffraction patterns (SAED), 40 μm size aperture was used.

Bulk chemical compositions of STO films were determined by x-ray photoelectron spectroscopy (XPS) using a Thermo Scientific K-Alpha spectrometer with a monochromatized Al Kα x-ray source. To reach the bulk film, 60 s ion milling process was applied with an Ar beam having an acceleration voltage of 1 kV.

Surface morphology of deposited films was recorded by using an atomic force microscope (AFM, Asylum Research MFP-3D) operating in tapping mode, and additionally, from FIB (FEI Vion Plasma FIB) measurements in which images were taken from top of the film surface.

Spectral transmission measurements were performed using a Carry 5000 ultraviolet-visible-near infrared (UV-VIS-NIR) double beam spectrophotometer in the wavelength range of 200–2000 nm relative to air. Film optical constants were extracted from ellipsometric measurements using a variable angle spectroscopic ellipsometer (V-VASE, J.A. Woollam Co., Inc.) for wavelengths ranging from 250 to 1000 nm. Film refractive indices (n) and extinction coefficients (k) of as-deposited and 300 °C annealed films were determined using the homogeneous Tauc-Lorentz (TL) while, graded TL function was used for films annealed >300 °C. All n and k in this paper correspond to the values at 550 nm. The absorption coefficient, $\alpha(\lambda) = 4\pi k(\lambda)/\lambda$, was calculated from $k(\lambda)$ values. The optical band gap energy (E_g) was evaluated using well-known Tauc formula.[27] The direct band gap values were determined from $(\alpha h\nu)^2$ vs $h\nu$ plots.

To evaluate electrical properties of noted STO films (STO-RT, STO-300 and STO-800), Ag/STO/p-Si(100) device structure has been fabricated on highly doped Si substrates. Top metal contacts were prepared by thermal evaporation (~80 nm thick Ag) followed with lift-off process. MIS capacitor structures with STO films as the insulating layers were fabricated on *p*-type Si(100) substrates at class 100 and 1000 cleanroom facilities. Ag and STO layers were patterned simultaneously to obtain MIS devices with 380.6 μm^2 active area during the development of AZ 5214E photoresist with AZ 400K developer (MicroChemicals GmbH) (AZ 400 K:H_2O = 1:4). Frequency-dependent dielectric properties of the fabricated test structures were measured using a semiconductor parameter analyzer (Keithley 4200-SCS), which is connected to a DC probe station (Cascade Microtech PM-5). Measurements were performed at 200 to 4 MHz frequency range under −1 V bias at RT with 30 mV rms voltage. The dielectric constants of the films were calculated from the parallel plate capacitance model $C = \varepsilon_0 \cdot \varepsilon \cdot A/t$ where C, t, ε_0, ε, and A correspond to the accumulation capacitance, film thickness, permittivity of free space (8.8542×10^{-12} F/m), dielectric constant of the film, and area of the electrodes (380.6 μm^2), respectively.[28] Dielectric losses of the selected samples were calculated from the formula G/Cω, G is the measured conductivity, C is the capacitance, ω is $2\pi f$, and here f is the frequency which is applied.[28] Before the frequency dependent capacitance measurement, capacitance voltage (C-V) characteristics of the selected samples were carried out for determination of the accumulation region of

TABLE I. Deposition conditions of RF-sputtered $SrTiO_3$ thin films.

Base pressure (mPa)	<0.87
Deposition pressure (Pa)	0.93
O_2/(O_2+Ar)	0/(0+30)
RF power (W)	100
Target size (mm)	50
Target to substrate holder distance (mm)	50
Deposition time (min)	20
Annealing temperature (°C) and time (h)	300, 600, 700, 800, and 900 for 1 h
Annealing time (min) for 700 °C	15, 30, 45 in O_2 flow

the selected samples. Accumulation region of the fabricated device is found to be at −1 V bias. Therefore, C-*f* measurements were performed at −1 V bias voltage.

III. RESULTS AND DISCUSSION

A. Film microstructure, composition and surface morphology

STO thin films were deposited on *p*-type Si(100) and quartz substrates at RT. GIXRD patterns of all as-deposited RT films only contained broadened feature, indicating that they were amorphous regardless of the deposition parameters (not presented here). In Figs. 1(a) and 1(b), XRD patterns of STO films are presented as a function of annealing temperature and annealing time, respectively. (012) reflection appeared after annealing at 300 °C as given in Fig. 1(a), which can be considered as a nanocrystalline phase of the STO films. Crystallization effect was visible for STO films with annealing temperature of 600 °C where (011), (111), (002), (012), (112), and (022) reflections were revealed. The other diffraction peaks of perovskite structure were not visible at spectra, which might be the result of insensitivity of GIXRD measurement to symmetric reflections. However, broad nanocrystal peak remained unchanged for the films annealed at this temperature.

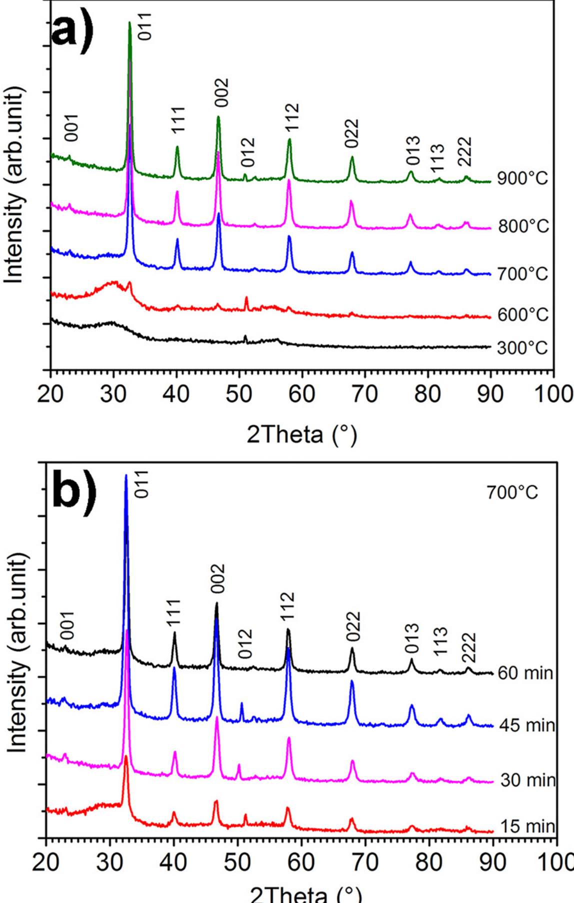

FIG. 1. (Color online) GIXRD patterns of STO thin films on *p*-Si(100) substrates (a) with different annealing temperatures (b) and annealing durations at 700 °C.

We noted that the crystallization of the films was observed at around 700 °C, besides annealing at 800 °C for 1 h caused further enhancement of the crystalline quality. The GIXRD patterns of STO films, annealed ≥700 °C, indicated that the films have polycrystalline cubic structure regardless of the composition giving the reflections for corresponding planes of (001) at 22.72°, (011) at 32.51°, (111) at 40.03°, (002) at 46.57°, (012) at 50.98°, (112) at 57.82°, (022) at 67.77°, (013) at 77.09°, (113) at 81.54°, and (222) at 85.91°, with the inorganic crystal structure database (ICSD) code (98-008-0873). For the annealed STO thin films, intensities of the diffraction peaks increased slightly and became stronger with annealing temperature up to 800 °C. In literature, XRD reflections of cubic STO crystal structure are stated at 22.78°, 32.43°, 40.00°, 46.52°, 52.40°, 57.85°, 67.91°, 72.65°, 77.28°, 81.83°, and 86.32°, for planes (001), (011), (111), (002), (012), (112), (022), (122), (013), (113), and (222), respectively. The significance of bulk $SrTiO_3$ crystallites with (122) peaks are not observed in our polycrystalline thin films in any postdeposition annealing temperature.

In Fig. 1(b), GIXRD peak profiles of polycrystalline STO thin films with different annealing durations for 700 °C annealing process are presented as an example. The time dependent annealing at 700 °C showed us that crystallization started in the first 15 min of the annealing process. Lattice parameter of the 700 °C annealed STO films is obtained from Rietveld refinement method and extracted as 3.9013, 3.9014, 3.9050, and 3.9054 Å, for 15, 30, 45, and 60 min annealing durations, respectively. Similarly, its value was found to be 3.9084 Å for 800 °C and 3.9060 Å for 900 °C annealing temperatures. As can be seen from analyses, the lattice parameter increased with annealing time and temperature. In addition, the unit cell volumes of the samples were calculated as 59.38, 59.38, 59.55, and 59.57 $Å^3$ for 700 °C 15, 30, 45, and 60 min annealing durations and 59.70 and 59.80 $Å^3$ for 800 and 900 °C annealing temperatures. The crystallite size of the films was calculated from Williamson-Hall plot for all samples in Figs. 2(a) and 2(b). The maximum crystallite size was observed as 28.9 nm for STO-800 sample, and it was lower for films annealed at 900 °C, ∼14.9 nm, due to recrystallization. Moreover, crystallite size increased from 7.8 to 20.6 nm with annealing time up to 45 min for films annealed at 700 °C, after 45 min annealing its value decreased to 15.1 nm and later increased to 19 nm for films annealed for 1 h.

In the present work, calculated crystallite size values of STO-800 and STO-700 samples for 30 min annealing time are comparable to the literature values of 20–30 nm.[29] However, other films showed lower crystallite size. This might be originating from lower deposition temperature.[30] It is known that different substrate temperatures and/or annealing temperatures produce different material characteristics.[31–35]

Survey and high-resolution XPS scans of STO films were recorded as a function of annealing temperature and time. The survey spectrum of STO samples revealed the presence of Sr, Ti, O, and Ar elements, where compositions are presented in Table II. All films showed oxygen deficiency. STO-RT sample was Sr rich with the Sr/Ti ratio of 1:4,

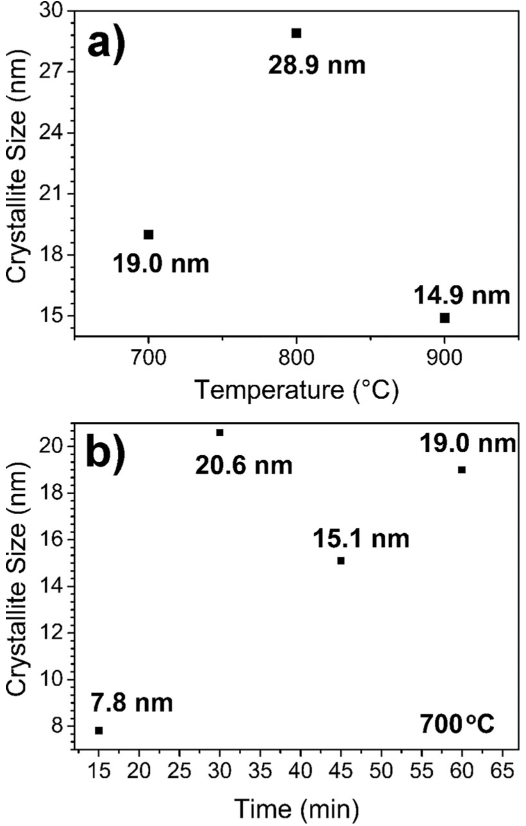

FIG. 2. Crystallite size of STO films on *p*-Si(100) substrate annealed at 700 °C as a function of (a) temperature and (b) time. Calculated from Williamson-Hall plot.

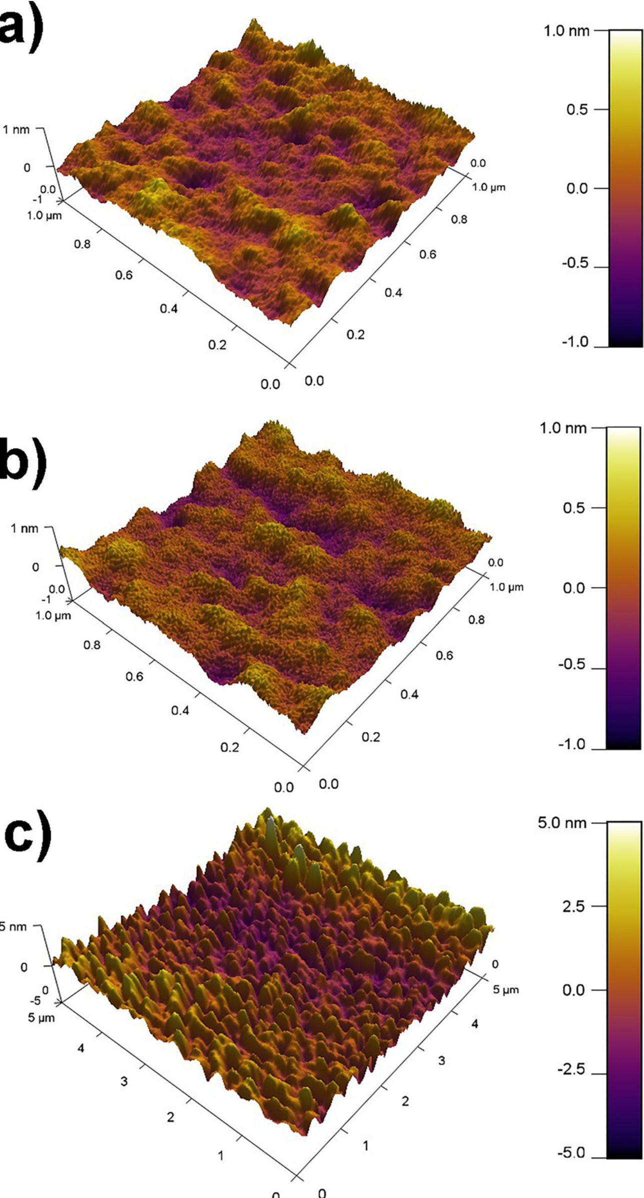

FIG. 3. (Color online) AFM images of amorphous and polycrystalline STO thin films on *p*-Si (100) substrates (a) as-deposited, rms: 0.17 nm, annealed at (b) 300 °C, rms: 0.16 nm, and (c) 800 °C, rms: 0.66 nm.

which was also found to be mainly amorphous. STO film annealed at 300 °C had nearly stoichiometric ratio of 1:1. However, no significant change was observed as a function of annealing time and temperature. In this study, composition of the STO films was determined after single etching step of 60 s by ion milling process.

The surface morphology and topology of STO thin films were investigated by AFM measurements. 1×1 and $5 \times 5\,\mu$m surface scans are taken from as-deposited and annealed STO films as presented in Fig. 3. STO-RT film image revealed a smooth surface with a uniform coating and a crack-free microstructure.

TABLE II. Sr, Ti, O, and Ar compositions of the as-deposited and annealed STO thin films as determined by XPS survey scans. Data were collected after 60 s of *in situ* Ar etching.

Sample name	Sr (at. %)	Ti (at. %)	O (at. %)	Ar (at. %)	Sr/Ti
STO-RT	22.66	16.52	56.58	4.24	1.4
STO-300	18.19	18.12	59.16	4.54	1.1
STO-600	22.87	19.02	54.88	3.22	1.2
STO-700/15	22.16	18.53	57.14	2.17	1.2
STO-700/30	23.01	17.98	56.69	2.32	1.3
STO-700/45	23.27	17.93	56.20	2.66	1.3
STO-700	23.08	19.68	54.09	3.15	1.2
STO-800	22.36	18.54	56.80	2.29	1.2
STO-900	20.25	22.30	54.39	3.07	0.9

However, the average rms surface roughness values increased as a function of annealing temperature from 0.17 nm (RT) to 0.98 nm (900 °C), which might be resulting from crystallite size increment. It is stated in the literature that surface roughness of the oxide thin films is mostly caused by oxygen vacancies.[32–34] In this study, surface roughness increase can be attributed to recrystallization process and oxygen vacancies as well as surface defects which is given in high resolution scanning electron microscope (HRSEM) image as a void formation.

Surface morphology of STO thin films was also examined by SEM measurements. Figure 4(a) shows plane and cross-section view SEM image for STO-800 thin film, deposited on Si(100) substrate at RT and annealed afterward at 800 °C for 1 h. Highly uniform and grainy structure with some voids were observed after annealing. As can be seen in figure, the

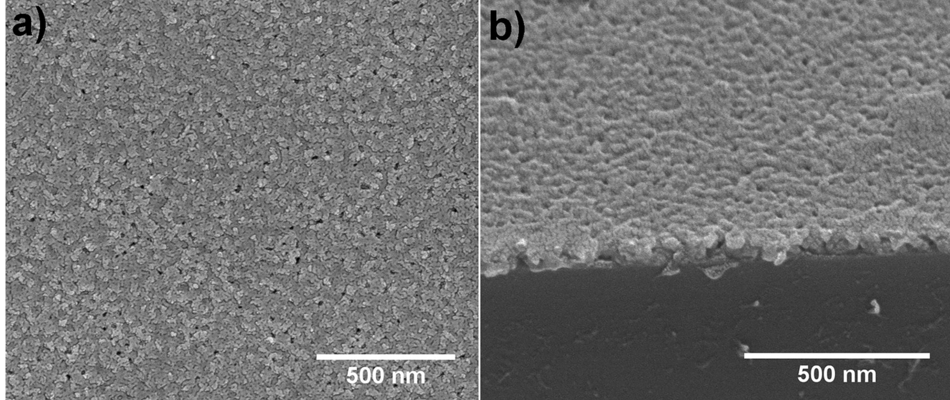

FIG. 4. HRSEM images of STO thin films annealed at 800 °C (a) plan view and (b) cross-section.

grain size distribution might be considered as relatively uniform. Average grain size values were estimated using IMAGE J software where grain boundaries were marked from the edges of the grains. Average diameter was calculated as ~15 nm. In Fig. 4(b), cross sectional image of STO-800 thin film is given in which the film thickness is measured as 80 nm. As-deposited films showed very smooth surface structure, whereas annealing at high temperatures (>700 °C) produced larger grains and void formation which might be related to the densification of the film. In this case, film densification and larger crystallite sizes could be one of the reasons for the increased surface roughnesses, and void formation.

TEM and HR-TEM images with SAED experiments were carried out on STO thin films annealed at 800 °C for further investigation of the crystal structure. Figure 5(a) shows the cross-sectional TEM image of STO-800 sample which depicts the interface of polycrystalline STO, SiO_2/Si substrate, and platinum coating on top, which is deposited to avoid sample damaging from FIB preparation process. The average thickness of STO thin film was measured as ~80 nm from cross-sectional TEM measurements, which is in close agreement with the thickness data obtained from SEM and ellipsometry measurements. A ~4 nm thick amorphous SiO_2 layer was observed at the STO/Si interface, which was present as native oxide on the surface of Si before the film growth. HR-TEM images which are shown in Fig. 5(b), as well as SAED pattern in Fig. 5(c), confirm the polycrystalline nature of STO film after 800 °C annealing. Polycrystalline diffraction rings of STO can be seen from the SAED patterns. The large bright spots on the diffraction pattern were related to the Si substrate, while the bright spots on the diffraction rings indicated STO crystalline planes. The interplanar spacing (d_{hkl}) values were calculated from the diffraction rings and the diffraction rings are indexed as (002), (112), and (111) reflections of cubic structure of polycrystalline STO which are supported by GIXRD results (ICSD reference code: 98-008-0873) (see Table III).

B. Optical properties

The effect of annealing on the optical properties such as refractive index (n), extinction coefficient (k), and optical band edge values (E_g) of films was studied by spectrophotometry and spectroscopic ellipsometry measurements. The optical transmission spectra of both as-deposited and annealed (300 and 900 °C in O_2) STO thin films, and the bare quartz substrate are given in Fig. 6, as an example.

As can be seen from these plots, all films were highly transparent ($k < 10^{-3}$). A significant decrease in the UV transmission was observed at wavelengths <350 nm for all films. Furthermore, the main absorption edge is shifted toward the higher wavelengths with increasing annealing temperature. The absorption edge shift might be attributed to improved crystallinity which is further confirming GIXRD results. Shift in the absorption edge is clearly observed for films annealed at 700 °C for 30 min (STO-700/30) and higher temperatures >700 °C. STO-800 and STO-900 films showed the lowest

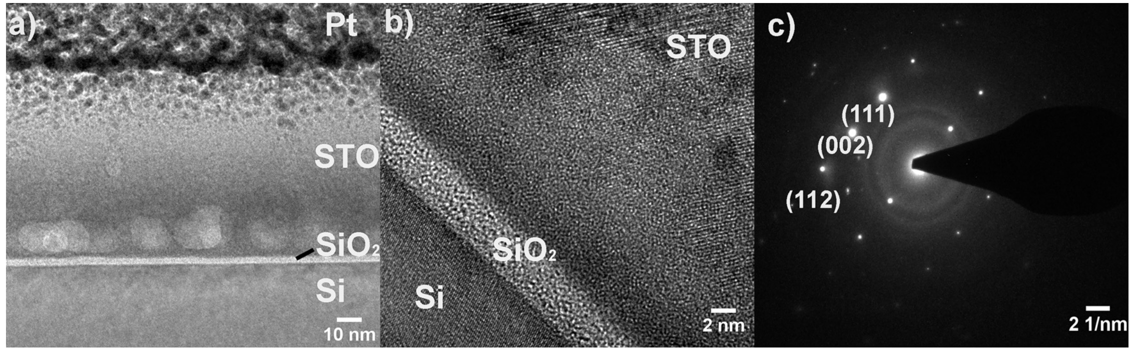

FIG. 5. (a) Cross-sectional TEM, (b) HR-TEM, and SAED images of the STO thin films annealed at 800 °C.

TABLE III. SAED results, theoretical values, and corresponding crystallographic planes.

	Interplanar spacing, d (Å)		
Diameter (1/nm)	Calculated	Theoretical[a]	Corresponding plane, *hkl*
5.076	1.970	1.9500	002
6.452	1.550	1.5926	112
8.157	2.260	2.2522	111

[a]Cubic STO, ICSD reference code: 98-008-0873.

optical transmittance in the visible region. The optical transmission spectra depend on three factors in general: oxygen deficiency, surface roughness, and impurity centers. In our films, the observed low optical transmission might be attributed to the higher surface roughness and void formation with annealing which can cause in higher reflection.

The dispersion curves of the as-deposited and annealed STO films were determined using spectroscopic ellipsometry measurements and the following data analysis. Tauc-Lorentz oscillator model was used for the determination of the optical constants, i.e., extinction coefficients and refractive indices. Figure 7 shows refractive indices of as-deposited and annealed STO films as a function of wavelength. No significant change was observed for films annealed $\leq$600 °C and $n(\lambda)$ values were in the range 1.79–1.82, whereas the films annealed at higher temperatures showed higher $n(\lambda)$ values and they were found to be in the range 1.90–2.16. The highest $n(\lambda)$ values were obtained for films annealed at 800 °C, which is close to the value of STO single crystal (2.39). It is a well-known fact that the refractive index increases with crystalline quality and this observation confirms this correlation. However, for the films annealed at 900 °C, lower n values were obtained compared to 800 °C annealed films, which might be related to recrystallization in thin films.[33,36] The summary of the refractive indices and extinction coefficients at 550 nm are presented in Table IV. The values determined for the STO thin films were found to be quite close to their counterparts.

The extinction coefficients (k) values, which were found to be ~zero, indicated that all films were absorption-free in

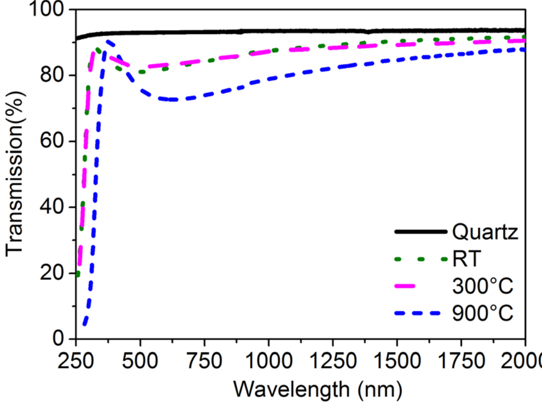

FIG. 6. (Color online) Transmission spectra of as-deposited and annealed STO thin films at 300 and 900 °C.

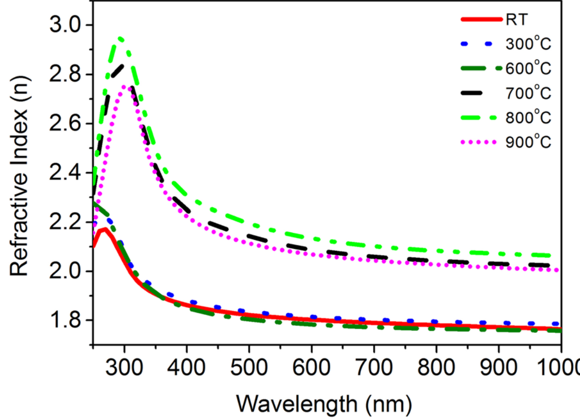

FIG. 7. (Color online) Spectral refractive indices of as-deposited and annealed STO films.

the measurement spectrum (see Fig. 6 and Table IV). Direct band gap energies (E_g) of all STO films were determined by Tauc equation as described in Sec. II. In Fig. 8, $(\alpha E)^2$ plot is presented as a function of energy for films annealed at 800 °C for 1 h. As can be seen from the plots, the E_g value of the film was ~4.18 eV. The optical band gap values of STO films decreased from 4.50 to 4.10 eV as a function of annealing temperature. The larger optical band gap observed for thin films compared to bulk STO (3.2 eV) might be attributed to strain-induced defects and/or amorphous structure due to the small crystallite size, which was estimated as 11–16 nm by the XRD analysis. In the literature, the optical band gap values are stated in the range of 3.32 to 3.80 eV (Ref. 32) and 4.25 eV (Ref. 33) for the polycrystalline STO films.

Furthermore, the optical band gap values of STO films annealed at 700 °C as a function of annealing time did not show significant change, and its value varied between 4.20 and 4.22 eV. However, the sharpness of the absorption edge in spectroscopic measurements (which is not shown here) increased with annealing time, indicating improved microstructure as it is anticipated.

C. Electrical properties

STO thin films are one of the attractive ferroelectric materials due to their high dielectric constant. In the present

TABLE IV. Summary of the refractive indices, extinction coefficient at 550 nm, and optical band gap values of the as-deposited and annealed STO thin films.

Sample name	n	k	E_g (eV)
STO-RT	1.81	0	4.50
STO-300	1.82	0	4.50
STO-600	179	0	4.55
STO-700/15	1.90	0	4.20
STO-700/30	2.15	0	4.22
STO-700/45	2.05	0	4.22
STO-700	2.11	0.002	4.20
STO-800	2.16	0.001	4.18
STO-900	2.09	0	4.10

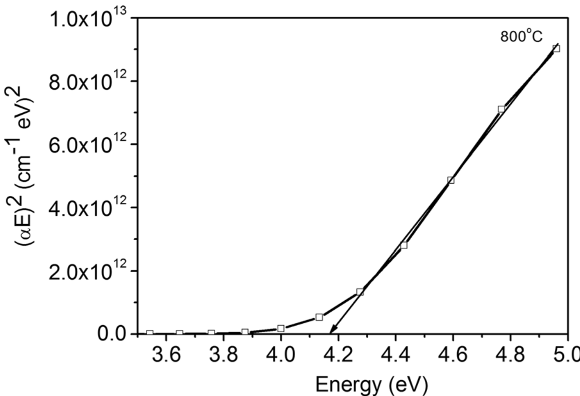

FIG. 8. $(\alpha E)^2$ vs E plot is presented for films annealed at 800 °C for 1 h, as example.

work, RT grown, 300 and 800 °C annealed STO films were chosen to reveal the dielectric constant and dielectric loss differences of amorphous, nanocrystalline, and polycrystalline STO thin films in MIS [Ag/STO/*p*-Si (100)] structure. Figures 9(a) and 9(b) show dielectric constants and dielectric loss values of as-deposited and annealed (at 300 and 800 °C) STO thin films as a function of frequency. Annealing at 300 and 800 °C for 1 h led to an increase in dielectric constant of films. As can be seen from plots, dielectric constants of STO-RT and STO-300 films were higher at lower frequencies compared to the higher frequencies. Dielectric constant of STO-RT films decreased gradually from 25 to 10 as a function of frequency up to 20 kHz, and stayed almost constant (~7) at higher frequencies. Dielectric constant values of STO-300 films also decreased from 40 to 7 as a function of frequency. The highest dielectric constant was obtained for polycrystalline STO-800 films. The dielectric constant of STO-800 films varied between 45 and 47 in the range of 1–3 MHz; however, above 3 MHz, its value decreased to 26. In our study, electrical characterization measurements were performed at RT. Morán *et al*. reported G(T) and R(T) measurements for thin layers of STO (2–30 nm) in $YBa_2Cu_3O_{7\text{-}x}$/SrTiO3/Au structures.[37] The resistivity of 4 nm STO was found between 2 and 13×10^6 Ω cm for RT to 4.2 K temperatures, respectively. G(T) measurements showed that conductivity is increasing with the STO barrier layer thickness which is in the range of 10^{-3} to 10^{-1} $\Omega^{-1}cm^{-1}$, for this study they have used 8, 20, and 30 nm STO layer, and temperatures were in the range of 4.2 to 300 K. In our study, frequency dependent conductivities G(*f*) of STO-RT, STO-300, and STO-800 are 2.59×10^{-3}, 1.45×10^{-3}, and 1.54×10^{-4} $\Omega^{-1}cm^{-1}$ at 1 kHz, respectively. However, with increasing frequency up to 4 MHz, conductivity drastically increased for STO-800 sample up to ~0.5 $\Omega^{-1}cm^{-1}$.

In Fig. 9(b), dielectric loss values are presented as a function of frequency for as-deposited and annealed films. As given in Fig. 9, RT grown films and 300 °C annealed films exhibited relatively higher loss values. On the contrary, the dielectric loss of the STO-800 films was lower (~0.02) up to 1 MHz. In STO-800 films, dielectric loss values increased sharply after 1 MHz and it reached to 2 at 4 MHz due to the conductivity (G) increment. It might be possible that the loss mechanism here mainly originates from the extrinsic loss mechanism. Charge defects move with AC electric field resulting from formation of the acoustic waves at the frequency of the applied field. Additionally, the reason of the high loss observed for polycrystalline STO-800 sample at high frequencies might be due to the local polar regions induced by various defects and structural imperfections which can be seen from SEM images.

In general, dielectric constant and loss values of STO thin films depend on many factors, i.e., annealing and measurement temperature, bottom electrodes, local polar regions, random field defects, composition, thickness, crystalline quality, etc.[5] In our work, small crystallite size, interface layer, and well known lattice mismatch between Si substrate and STO might be the reason for the observed low dielectric constant in STO thin films compared to the reported dielectric constants. It is known that the difference between the thermal expansion coefficient values of STO thin film and Si substrates can cause lattice disorder in the films and hence stress.[33] Furthermore, as it was noted by Radhakrishnan *et al*. that the thickness of the film is another important parameter for the determination of the dielectric constant, they showed that STO films with a thickness <100 nm show significantly lower dielectric constant values.[2]

In recent years, epitaxial growth of oxide films attracted the attention since a perfect control of the interface could be

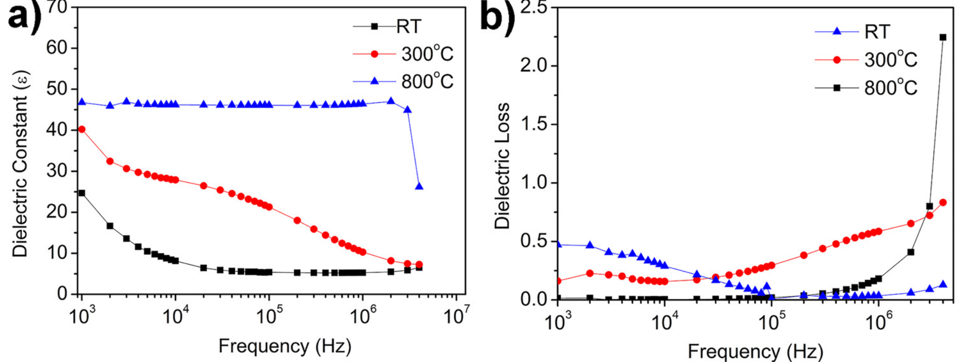

FIG. 9. (Color online) (a) Dielectric constants and (b) dielectric loss values of as-deposited and annealed (at 300 and 800 °C) STO thin films as a function of frequency.

obtained and combined with better crystallinity. Epitaxial films are grown by several techniques, including MBE and sputtering using buffer layers.[38,39] Fuchs *et al*. deposited epitaxial grown 200–500 nm STO films with (100) growth orientation by magnetron sputtering on $YBa_2Cu_3O_{7-x}$ electrodes.[38] They investigated the temperature dependent electrical properties of epitaxial grown STO films. The dielectric constant of those films was ~5000 at 90 K; even with the increased temperatures up to RT, ε values were still high around 1000. They also noted frequency dependent dielectric constant measurement of epitaxial STO films between the frequency range of $10–10^6$ ω (s^{-1}) and the dielectric constant values decreased with the increasing frequency from 8000 to 1000. Although the epitaxial grown films have better crystallinity and higher dielectric constants, present dielectric and dielectric loss values of the STO films with a thickness of <100 nm are promising for future microelectronic applications. For example, several metal oxide materials, including HfO_2 and ZrO_2, are alternatives to reduce the equivalent gate oxide thickness of the metal oxide semiconductor field effect transistors; however, they become polycrystalline during thermal treatments carried out in the device processes, thus leading to possible formation of leakage channels at grain boundaries. However, STO thin films are stable up to high temperatures compared to their counterparts and have relatively higher temperature stability. Yadav and Ghosh recently reported that amorphous STO films can be used in transparent and flexible organic field effect transistor as a gate dielectric material.[40] They used STO thin films with a dielectric constant values in the range 10–30, and promising application in microelectronics.

IV. SUMMARY AND CONCLUSIONS

We have studied the effect of annealing on structure, composition, morphology, and of the optical and electrical properties of STO films as a function of annealing temperature, and annealing time. Highly transparent films with excellent adhesion were deposited using RF sputtering system. Sr/Ti compositions of films ranging from 0.9 to 1.4 were obtained by changing the RT deposition to annealing temperature. The as-deposited films were amorphous, and the films annealed at 300 °C contained nanocrystalline phase. Postdeposition annealing at 600 °C for 1 h promoted nanocrystallization and further annealing at 700 °C resulted crystallization into the perovskite phase. Stoichiometric STO films which were annealed at 300 °C for 1 h was amorphous and Sr-rich STO films (≥700 °C for ≥15 min annealed) exhibited a certain degree of (011) texture while the slightly Ti-rich STO films (900 °C 1 h annealed) showed recrystallization. The calculated crystallite size slightly decreased upon annealing at 900 °C, and it significantly affected the optical and electrical characteristics of the films. Transparency of all annealed and as-deposited films was about 80% in the UV-VIS and the NIR regions and they exhibited an increased optical loss due to light scattering with annealing. The refractive index value increased from 1.82 to 2.16 with annealing, and the optical band gap values were decreased from 4.50 to 4.10 eV, indicating densification and improved film structure. Similarly, films annealed at 800 °C showed high dielectric constant values compared to their as-deposited and low temperature annealed counterparts. Furthermore, films annealed at 800 °C showed stable dielectric constant values ~ 46 up to 3 MHz but it drastically decreased to 27 after this frequency.

Although the calculated dielectric constants are relatively lower than reported values for microelectronic applications in the literature. The crystallinity improves at high temperatures with annealing, but the annealing at 800 °C is not enough to get textured films with thickness <100 nm. This study indicates that postdeposition annealing temperature and annealing time have considerable influence on the structural, optical, and electrical properties of RT sputtered amorphous grown STO thin films.

ACKNOWLEDGMENTS

This work was performed at UNAM–Institute of Materials Science and Nanotechnology. E.G. gratefully acknowledges the financial support from TUBITAK (1001 Project No. 115F077). The authors thank Shahid Ali Leghari, and Mustafa Guler for their assistance with AFM and TEM measurements.

[1]A. K. Tagantsev, V. O. Sherman, K. F. Astafiev, J. Venkatesh, and N. Setter, J. Electroceram. **11**, 5 (2003).
[2]K. Radhakrishnan, C. L. Tan, H. Q. Zheng, and G. I. Ng, J. Vac. Sci. Technol. **18**, 1638 (2000).
[3]K. Morito, H. Wakabayashi, T. Suzuki, and M. Fujimoto, J. Ceram. Soc. Jpn. **110**, 408 (2002).
[4]J. H. Lee, Y. J. Cho, Y. S. Min, D. Kim, and S. W. Rhee, J. Vac. Sci. Technol. **20**, 1828 (2002).
[5]H. Nili, S. Walia, S. Balendhran, D. B. Strukov, M. Bhaskaran, and S. Sriram, Adv. Funct. Mater. **24**, 6741 (2014).
[6]H. Nili *et al.*, Adv. Funct. Mater. **25**, 3172 (2015).
[7]J. F. Scott and A. P. A. Carlos, Science **246**, 1400 (1989).
[8]P. C. Joshi and S. B. Krupanidhi, J. Appl. Phys. **73**, 7627 (1993).
[9]W. Lee, J. H. Han, W. Jeon, Y. W. Yoo, S. Woon Lee, S. K. Kim, C.-H. Ko, C. Lansalot-Matras, and C. S. Hwang, Chem. Mater. **25**, 953 (2013).
[10]H. J. Choi, S. W. Park, G. D. Han, J. Na, G.-T. Kim, and J. H. Shim, Appl. Phys. Lett. **104**, 242105 (2014).
[11]Y. Kanemitsu and Y. Yamada, Phys. Status Solidi B **248**, 416 (2011).
[12]D. Kan *et al.*, Nat. Mater. **4**, 816 (2005).
[13]H. Takashima, K. Shimada, N. Miura, T. Katsumata, Y. Inaguma, and K. Ueda, Adv. Mater. **21**, 3699 (2009).
[14]A. E. Souza, G. T. A. Santos, B. C. Barra, W. D. Macedo, Jr., S. R. Teixeira, C. M. Santos, A. M. O. R. Senos, L. Amaral, and E. Longo, Cryst. Growth Des. **12**, 5671 (2012).
[15]N. Setter *et al.*, J. Appl. Phys. **100**, 051606 (2006).
[16]A. Roelofs, T. Schneller, K. Szot, and R. Waser, Nanotechnology **14**, 250 (2003).
[17]A. Rüdiger, T. Schneller, A. Roelofs, S. Tiedke, T. Schmitz, and R. Waser, Appl. Phys. A **80**, 1247 (2005).
[18]A. Kosola, M. Putkonen, L. S. Johansson, and L. Niinistö, Appl. Surf. Sci. **211**, 102 (2003).
[19]L. Zhang and R. Engel-Herbert, Phys. Status Solidi RRL **8**, 917 (2014).
[20]L. S. Peng and B. H. Moeckly, J. Vac. Sci. Technol., A **22**, 2437 (2004).
[21]W. Wu, K. H. Wong, C. L. Mak, G. Pang, C. L. Choy, and Y. Zhang, J. Vac. Sci. Technol., A **18**, 2378 (2000).
[22]M. D. McDaniel, A. Posadas, T. Q. Ngo, A. Dhamdhere, D. J. Smith, A. A. Demkov, and J. G. Ekerdt, J. Vac. Sci. Technol. **31**, 01A136 (2013).
[23]B. D. Cullity and S. R. Stock, *Elements of X-ray Diffraction*, 3rd ed. (Prentice-Hall, Upper Saddle River, NJ, 2001), pp. 170, 619.
[24]T. Degen, M. Sadki, E. Bron, U. König, and G. Nenert, J. Powder Diffr. **29**, S13 (2014).

[25]H. M. Rietveld, Acta Cryst. **22**, 151 (1967).
[26]H. M. Rietveld, J. Appl. Cryst. **2**, 65 (1969).
[27]K. van Benthem, C. Elsässer, and R. H. French, J. Appl. Phys. **90**, 6156 (2001).
[28]Z. Wang, V. Kugler, U. Helmersson, N. Konofaos, E. K. Evangelou, S. Nakao, and P. Jin, Appl. Phys. Lett. **79**, 1513 (2001).
[29]B. A. Baumert *et al.*, J. Appl. Phys. **82**, 2558 (1997).
[30]B. Kınacı, N. Akın, İ. Kars Durukan, T. Memmedli, and S. Özçelik, Superlattice Microstruct. **76**, 234 (2014).
[31]Y. Gao, Y. Masuda, and K. Koumoto, J. Korean Ceram. Soc. **40**, 213 (2003).
[32]G. Panomsuwan, O. Takai, and N. Saito, J. Mater. Eng. Perform. **22**, 863 (2013).
[33]E. Goldenberg, T. Bayrak, C. Ozgit-Akgun, A. Haider, S. A. Leghari, M. Kumar, and N. Biyikli, Thin Solid Films **590**, 193 (2015).
[34]F. S. Aguirre-Tostado, A. Herrera-Gomez, J. C. Woicik, R. Droopad, Z. Yu, D. G. Schlom, J. Karapetrova, P. Zschack, and P. Pianetta, J. Vac. Sci. Technol. **22**, 1356 (2004).
[35]M. Gulen, G. Yildirim, S. Bal, A. Varilci, I. Belenli, and M. Oz, J. Mater. Sci. Mater. Electron. **24**, 467 (2013).
[36]E. Çetinörgü-Goldenberg, J. E. Klemberg-Sapieha, and L. Martinu, Appl. Opt. **51**, 6498 (2012).
[37]O. Morán, R. Hott, and D. Fuchs, Thin Solid Films **517**, 1908 (2009).
[38]D. Fuchs, C. W. Schneider, R. Schneider, and H. Rietschel, J. Appl. Phys. **85**, 7362 (1999).
[39]G. Delhaye, C. Merckling, M. El-Kazzi, G. Saint-Girons, M. Gendry, Y. Robach, G. Hollinger, L. Largeau, and G. Patriarche, J. Appl. Phys. **100**, 124109 (2006).
[40]S. Yadav and S. Ghosh, ACS Appl. Mater. Interfaces **8**, 10436 (2016).